Langmuir Article

pubs.acs.org/Langmuir

Self-Assembly of ABC Star Triblock Copolymer Thin Films Confined with a Preferential Surface: A Self-Consistent Mean Field Theory

Bo Lin, Hongdong Zhang,* Feng Qiu,* and Yuliang Yang

Key Laboratory of Molecular Engineering of Polymer, Ministry of Education, and Department of Macromolecular Science, Fudan University, Shanghai 200433, China

Received June 22, 2010. Revised Manuscript Received October 24, 2010

The microphase separation and morphology of a nearly symmetric $A_{0.3}B_{0.3}C_{0.4}$ star triblock copolymer thin film confined between two parallel, homogeneous hard walls have been investigated by self-consistent mean field theory (SCMFT) with a pseudospectral method. Our simulation experiments reveal that under surface confinement, in addition to the typically parallel, perpendicular, and tilted cylinders, other phases such as lamellae, perforated lamellae, and complex hybrid phases have been found to be stable, which is attributed to block−substrate interactions, especially for those hybrid phases in which A and B blocks disperse as spheres and alternately arrange as cubic CsCl structures, with a network preferred structure of C block. The results show that these hybrid phases are also stable within a broad hybrid region (H region) under a suitable film thickness and a broad field strength of substrates because their free energies are too similar to being distinguished. Phase diagrams have been evaluated by purposefully and systematically varying the film thickness and field strength for three different cases of Flory−Huggins interaction parameters between species in the star polymer. We also compare the phase diagrams for weak and strong preferential substrates, each with a couple of opposite quality, and discuss the influence of confinement, substrate preference, and the nature of the star polymer on the stability of relatively thinner and thick film phases in this work.

1. Introduction

The self-assembly of block copolymers in confined space and its microphase separation has attracted increasing amounts of attention in the field of soft condensed matter physics, biophysics, nanoscale materials, and nanotechnology.[1,2] Geometric confinement is one of the alternative methods of fabricating novel nanoscale-ordered structures by simply changing the composition, interaction parameters between different immiscible species, and bulk architecture of the block copolymers.[3]

Block copolymers are composed of polymerized sequences or distinct polymer blocks as repeat units jointed chemically at their ends, including AB diblock, ABA linear, ABC linear, and ABC star triblock copolymers or other types of multiblock copolymers.[4,5] If the chemically distinct blocks are immiscible, then the excess free energy will discourage mixing; in the meantime, these thermodynamic forces are balanced by entropic constraints on the long-chain molecules, which can effectively prevent macrophase separation of different species, and these molecules can self-assemble into a variety of thermodynamically stable and ordered nanoscale morphologies such as the three-color lamellae phase (LAM_3), a hexagonal lattice phase (HEX), two interpenetrating tetragonal lattice phase (TET_2), and body-centered cubic spheres (BCC) and other complex structures such as a lamellae phase with beads inside or at the interface (LAM + BD) and gyroids (G) in melts and solutions.[5−9] Because of this ability to assemble, block copolymers are deemed to be versatile material candidates for many applications in bulk materials and thin films with different geometrical structures.[5] In comparison to the phase structure of the bulk, a confinement system of a thin film places a more distinct constraint on the morphology and phase behavior of block copolymers. Furthermore, the thin film of a block copolymer under confinement demonstrates much more complicated structures that are attributed to the domain spacing of the structures, which is quite different from the bulk, and the preferential surface field can induce the polymer blocks to segregate near the surface of the substrates. By choosing a suitable geometry confinement and the interactions between polymers and substrates, a large-scale alignment of surface reconstruction and a series of complex morphologies can be obtained in thin films.[8,10,11]

In recent years, many studies have focused on the block copolymer system under various confinements such as thin films,[4,10−15] cylindrical pores,[3,16−18] spheres,[19] and multiple phase systems for the

*Corresponding authors. Tel: +86-21-65642125. E-mail: zhanghd@fudan.edu.cn, zhanghongdong@gmail.com (H.Z.); fengqiu@fudan.edu.cn (F.Q.).

(1) Matsen, M. W. *J. Phys.: Condens. Matter* **2002**, *14*, R21–R47.
(2) Park, M.; Harrison, C.; Chaikin, P. M.; Register, R. A.; Adamson, D. H. *Science* **1997**, *276*, 1401–1404.
(3) Xu, Y. C.; Li, W. H.; Qiu, F.; Yang, Y. L. *J. Phys. Chem. B* **2009**, *113*, 11153–11159.
(4) Yang, Y. Z.; Qiu, F.; Zhang, H. D.; Yang, Y. L. *Polymer* **2006**, *47*, 2205–2216.
(5) Khanna, V.; Cochran, E. W.; Hexemer, A.; Stein, G. E.; Fredrickson, G. H.; Kramer, E. J.; Li, X.; Wang, J.; Hahn, S. F. *Macromolecules* **2006**, *39*, 9346–9356.
(6) Bates, F. S.; Fredrickson, G. H. *Annu. Rev. Phys. Chem.* **1990**, *41*, 525–557.
(7) Bates, F. S.; Fredrickson, G. H. *Phys. Today* **1999**, *52*, 32–38.
(8) Han, W. C.; Tang, P.; Li, X.; Qiu, F.; Zhang, H. D.; Yang, Y. L. *J. Phys. Chem. B* **2008**, *112*, 13738–13748.
(9) Tang, P.; Qiu, F.; Zhang, H. D.; Yang, Y. L. *J. Phys. Chem. B* **2004**, *108*, 8434–8438.
(10) Kellogg, G. J.; Walton, D. G.; Mayes, A. M.; Lambooy, P.; Russell, T. P.; Gallagher, P. D.; Satija, S. K. *Phys. Rev. Lett.* **1996**, *76*, 2503–2506.
(11) Walton, D. G.; Kellogg, G. J.; Mayes, A. M.; Lambooy, P.; Russell, T. P. *Macromolecules* **1994**, *27*, 6225–6228.
(12) Matsen, M. W. *J. Chem. Phys.* **1997**, *106*, 7781–7791.
(13) Wang, Q.; Yan, Q. L.; Nealey, P. F.; de Pablo, J. J. *J. Chem. Phys.* **2000**, *112*, 450–464.
(14) Huinink, H. P.; Brokken-Zijp, J. C. M.; van Dijk, M. A.; Sevink, G. J. A. *J. Chem. Phys.* **2000**, *112*, 2452–2462.
(15) Wang, Q.; Nealey, P. F.; de Pablo, J. J. *Macromolecules* **2001**, *34*, 3458–3470.
(16) Sevink, G. J. A.; Zvelindovsky, A. V.; Fraaije, J.; Huinink, H. P. *J. Chem. Phys.* **2001**, *115*, 8226–8230.
(17) Li, W. H.; Wickham, R. A.; Garbary, R. A. *Macromolecules* **2006**, *39*, 806–811.

inclusion of filler particles[20] to control the morphology and explore new phases. However, the phase behavior of ABC triblock copolymers, especially for those with three different blocks, become more intricate than that of two-component systems such as the AB diblock[4,10−15] and the symmetric ABA block copolymer.[21,22] There are too many parameters involved in the film of the three-component system to establish an overall research system. The preferentially perpendicular lamellae, a typical phase of ABC linear triblock copolymers, had been found under confinement with two attractive walls for the middle block of polymer by means of self-consistent mean field theory (SCMFT).[23] The ABC linear film confined with two chemically identical walls under symmetric interactions of different species was also studied via the strong segregation limit in SCMFT.[24] Microphase separation of the thin film for the ABC linear triblock copolymers investigated by Monte Carlo simulations (MC) was affected by the composition of the polymer and the interactions between different species.[25] The simulation results of MC for the cylindrical thin film also showed that there are different transformations among parallel cylinders, perpendicular cylinders, and distorted mixed structures in the asymmetric ABC linear polymer.[26] Moreover, the bulk of the linear triblock copolymer studied by Ludwigs demonstrated an interesting core−shell gyroid structure in their mesoscale calculations and experiments.[27,28]

Nevertheless, a nonlinear polymer is quite different from a linear one, such as the star triblock copolymer intensively studied by Gemma,[29] Liang,[30] and Qiu,[9] who had reported a thermodynamically stable microphase in various shapes such as flat lamellae and a complex lamellae phase with a cylinder, a hexagonal lattice, and a core−shell hexagonal lattice. Meanwhile, hexagonal honeycomb and polygon phases were also found by changing the volume fractions of the species in the star polymer, which revealed that the molecular architecture of the polymer chain imposed a strong topological constraint on the microphase geometry.

The confined thin films of block copolymers have been extensively studied in experiments as well, such as that used as an attractive template for the production of nanostructures and in nanolithography, because of their ability to self-assemble on certain length scales. Herein, it is essential to the proper design and processing of these film materials, especially with respect to controlling the morphology and orientation of the nanodomains over macroscopic length scales.[5] Krishnan used an underwater surface reconstruction technique to self-assemble thin films of comblike diblock copolymers polystyrene-*b*-poly(ethylene glycol), which was expected to be used to explore cylindrical and spherical microphases with a driving force of surface segregation.[31]

Rodwogin explored thin films of polylactide−poly(dimethylsiloxane)−polylactide (PLA−PDMS−PLA) triblock copolymers as multifunctional nanolithographic templates. They demonstrated the formation of well-ordered arrays of hexagonally packed PDMS cylinders oriented normal to the substrate. Nevertheless, the incorporation of inorganic domains into such block copolymers provides etch contrast that can potentially reduce processing times and costs in nanolithographic applications.[32] Khanna investigated the effect of surface energy and chain architecture on the orientation of microdomains in relatively thick (600−800 nm) films of block copolymers of poly(cyclohexylethylene) (C) and poly(ethylene) (E), and they found that the linear cylinder and lamellae CEC triblock copolymers orient their microdomains normal to the surface throughout the film thickness, comparing the parallel orientation of a lamellar E-rich surface layer for the bulk of the lamellar CE diblock copolymer. The orientated parallel film of triblock copolymer was stabilized on the condition that the midblock has a lower surface energy and the difference in surface energy of the two blocks is large enough to compensate for this conformational penalty, which is absent in diblock copolymers.[5]

However, the experimental techniques involved in patterning substrates with chemical or physical features on the macroscopic length scale require sophisticated and costly processing, let alone the complicated chain architecture of a star triblock copolymer. In this regard, computer simulation plays a convenient and effective role in guiding the experiments and developing novel film materials.[33]

Self-consistent mean field theory (SCMFT), as one of the most successful theoretical methods, is very effective in investigating the equilibrium phases in block copolymers and plays a major role in establishing the bulk phase diagram for different block copolymers.[3,4,8,9] On the basis of confined self-assembly, thin film of block copolymers have presented many interesting structures with various confinement effects compared with bulk block copolymers, and until now, only a few theoretical studies have been conducted on the self-assembly of star triblock copolymers confined thin films. It is fascinating for us to study star triblock copolymer films under surface confinement. Therefore, in the present work, we employ SCMFT to evaluate the morphology and phase behavior of thin films for ABC star triblock copolymers confined between two homogeneous, parallel substrates. Equilibrium microstructures are explored for various morphologies, and their stability regions as a function of film thickness and field strength for three different cases of appointed Flory−Huggins interaction parameters are identified by comparing their minimal free energy.

The remainder of the article is organized as follows. In section 2, we start with a brief description of the theoretical model and the specific application for thin films of star triblock copolymers. In section 3, we present the morphology and the phase diagram of the confined films with various block−substrate interactions. Section 4 is devoted to the main conclusions in this work.

2. Theoretical Method

The SCMFT for the bulk and confined triblock copolymers has already been developed. In this section, we briefly describe the SCMFT simulation method employed to predict the equilibrium structure of a confined film for ABC star triblock copolymers. We consider a system of n ABC star triblock copolymer melts with a volume V. Each copolymer has A, B, and C arms that are joined at a central core (junction point) as shown in Scheme 1, and the melt

(18) Yu, B.; Sun, P. C.; Chen, T. H.; Jin, Q. H.; Ding, D. T.; Li, B. H.; Shi, A. C. *J. Chem. Phys.* **2007**, *127*, 114906.
(19) He, X. H.; Song, M.; Liang, H. J.; Pan, C. Y. *J. Chem. Phys.* **2001**, *114*, 10510–10513.
(20) Lee, J. Y.; Shou, Z. Y.; Balazs, A. C. *Macromolecules* **2003**, *36*, 7730–7739.
(21) Horvat, A.; Lyakhova, K. S.; Sevink, G. J. A.; Zvelindovsky, A. V.; Magerle, R. *J. Chem. Phys.* **2004**, *120*, 1117–1126.
(22) Matsen, M. W. *Curr. Opin. Colloid Interface Sci.* **1998**, *3*, 40–47.
(23) Pickett, G. T.; Balazs, A. C. *Macromol. Theory Simul.* **1998**, *7*, 249–255.
(24) Chen, H. Y.; Fredrickson, G. H. *J. Chem. Phys.* **2002**, *116*, 1137–1146.
(25) Feng, J.; Ruckenstein, E. *Polymer* **2002**, *43*, 5775–5790.
(26) Chen, P.; Liang, H. J. *J. Phys. Chem. B* **2006**, *110*, 18212–18224.
(27) Ludwigs, S.; Krausch, G.; Magerle, R.; Zvelindovsky, A. V.; Sevink, G. J. A. *Macromolecules* **2005**, *38*, 1859–1867.
(28) Ludwigs, S.; Schmidt, K.; Stafford, C. M.; Amis, E. J.; Fasolka, M. J.; Karim, A.; Magerle, R.; Krausch, G. *Macromolecules* **2005**, *38*, 1850–1858.
(29) Gemma, T.; Hatano, A.; Dotera, T. *Macromolecules* **2002**, *35*, 3225–3237.
(30) Kou, D. Z.; Jiang, Y.; Liang, H. J. *J. Phys. Chem. B* **2006**, *110*, 23557–23563.
(31) Krishnan, S.; Paik, M. Y.; Ober, C. K.; Martinelli, E.; Galli, G.; Sohn, K. E.; Kramer, E. J.; Fischer, D. A. *Macromolecules* **2010**, *43*, 4733–4743.
(32) Rodwogin, M. D.; Spanjers, C. S.; Leighton, C.; Hillmyer, M. A. *ACS Nano* **2010**, *4*, 725–732.
(33) Yang, G.; Tang, P.; Yang, Y.; Cabral, J. T. *J. Phys. Chem. B* **2009**, *113*, 14052–14061.

Scheme 1. Molecular Architecture of an ABC Star Triblock Copolymer

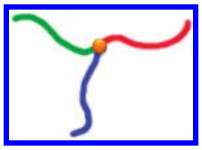

system is confined between two hard, flat walls with a distance between them of Λ. The total degree of polymerization of the star block is N, and the A, B, and C blocks consist of f_AN, f_BN, and f_CN monomers, respectively. We scale distances by the Gaussian radius of gyration $R_g = a(N/6)^{1/2}$ and assume that the A, B, and C segments have equal monomer statistical Kuhn lengths of $a = 1$. The bulk monomer density ρ is assumed to be the same for all chemical species. To deal with a many-body system, one considers the statistics of a single copolymer chain in a set of effective chemical potential fields $\omega_i(\vec{r})$, where i represents block species A, B, and C. Self-consistent mean field theory conjugated to local segment densities is introduced

$$\omega_A(\vec{r}) = \chi_{AB}N\phi_B(\vec{r}) + \chi_{AC}N\phi_C(\vec{r}) - H(\vec{r})N + \xi(\vec{r}) \quad (1)$$

$$\omega_B(\vec{r}) = \chi_{AB}N\phi_A(\vec{r}) + \chi_{BC}N\phi_C(\vec{r}) + H(\vec{r})N + \xi(\vec{r}) \quad (2)$$

$$\omega_C(\vec{r}) = \chi_{AC}N\phi_A(\vec{r}) + \chi_{BC}N\phi_B(\vec{r}) + H(\vec{r})N + \xi(\vec{r}) \quad (3)$$

With a surface field of $H(\vec{r})N$,

$$H(\vec{r}) = \begin{cases} \frac{1}{4}\Lambda_1\left(1+\cos\left(\frac{\pi z}{\varepsilon}\right)\right), & 0\le z\le\varepsilon \\ 0, & \varepsilon\le z\le\Delta-\varepsilon \\ \frac{1}{4}\Lambda_2\left(1+\cos\left(\frac{\pi z}{\varepsilon}\right)\right), & \Delta-\varepsilon\le z\le\Delta \end{cases} \quad (4)$$

z is the coordinate perpendicular to the film, ε denotes the thickness of the surface, and Λ_1 and Λ_2 are block−substrate interactions that control the strength of the interaction between the polymer block and the substrate at the $z = 0$ and Δ surfaces. We assume that positive Λ_1 and Λ_2 represent the A-attractive wall and negative Λ_1 and Λ_2 represent the A-repellant surface wall.

In eqs 1−3, ϕ_A, ϕ_B, and ϕ_C are the local densities of species A, B, and C, respectively. χ_{ij} is the Flory−Huggins interaction parameter between different species $i$and$j$. $\xi(\vec{r})$ is the field that ensures incompressibility, which is determined by

$$\phi_A(\vec{r}) + \phi_B(\vec{r}) + \phi_C(\vec{r}) = \phi(\vec{r}) \quad (5)$$

In the bulk, $\phi(\vec{r})$ always equals 1, independent of position $\vec{r}$. Near the confined boundaries, from the melt to the hard walls, $\phi(\vec{r})$ decays from 1 to 0. To simplify the calculation, we define it to be $^1/_2$ in the surface layers,

$$\phi(z) = \begin{cases} \frac{1}{2}, & 0\le z\le\varepsilon \\ 1, & \varepsilon\le z\le\Delta-\varepsilon \\ \frac{1}{2}, & \Delta-\varepsilon\le z\le\Delta \end{cases} \quad (6)$$

Therefore, the value of $H(\vec{r})$ is

$$H(\vec{r}) = \begin{cases} \frac{1}{4}\Lambda_1, & 0\le z\le\varepsilon \\ 0, & \varepsilon\le z\le\Delta-\varepsilon \\ \frac{1}{4}\Lambda_2, & \Delta-\varepsilon\le z\le\Delta \end{cases} \quad (7)$$

In SCMFT, the free energy of the system F can be written as

$$\begin{aligned} \frac{F}{nk_BT} = & -\ln\left(\frac{Q}{V}\right) + \frac{1}{V}\int d^3\vec{r}\,\chi_{AB}N\phi_A(r)\,\phi_B(\vec{r}) \\ & + \frac{1}{V}\int d^3\vec{r}\,\chi_{AC}N\phi_A(\vec{r})\,\phi_C(\vec{r}) \\ & + \frac{1}{V}\int d^3\vec{r}\,\chi_{BC}N\phi_B(\vec{r})\,\phi_C(r) \\ & - \frac{1}{V}\int d^3\vec{r}\,[\omega_A(\vec{r})\,\phi_A(\vec{r}) + \omega_B(\vec{r})\,\phi_B(\vec{r}) + \omega_C(\vec{r})\,\phi_C(\vec{r})] \\ & - \frac{1}{V}\int d^3\vec{r}\,\xi(\vec{r})[\phi_0(r) - \phi_A(\vec{r}) - \phi_C(\vec{r})] \\ & - \frac{1}{V}\int d^3\vec{r}\,H(\vec{r})[\phi_A(\vec{r}) - \phi_B(\vec{r}) - \phi_C(\vec{r})] \end{aligned} \quad (8)$$

where $Q = \int q_i(s,\vec{r})\,q_i^+(s,\vec{r})\,d\vec{r}$ is the partition function of a single triblock copolymer chain in the surface field $H(\vec{r})$ and can be obtained by the polymer segment distribution functions $q_i(s,\vec{r})$ and $q_i^+(s,\vec{r})$ for a single chain of contour length s with its end segment at position $\vec{r}$. Each star triblock copolymer chain is parametrized with the variable s, increasing continuously from 0 to 1 along each arm of the star polymer, which begins at the core (junction point) of the star polymer $s = 0$ and ends at the terminal of each arm of the star polymer $s = 1$. $q_i(s,\vec{r})$ and $q_i^+(s,\vec{r})$ satisfies and can be solved by the following two modified diffusion equations

$$\frac{\partial}{\partial s}q_i(s,\vec{r}) = \frac{Na^2}{6}\nabla^2 q_i(s,\vec{r}) - \omega_i q_i(s,\vec{r}) \quad (9)$$

$$\frac{\partial}{\partial s}q_i^+(s,\vec{r}) = -\frac{Na^2}{6}\nabla^2 q_i^+(s,\vec{r}) + \omega_i q_i^+(s,\vec{r}) \quad (10)$$

with $q_i^+(s,\vec{r})$ being another segment distribution function because the two arbitrary terminals of the triblock copolymer are completely different. The initial conditions of the above diffusion equations are $q_i(0,\vec{r}) = q_j^+(0,\vec{r})\,q_k^+(0,\vec{r})$ and $q_i^+(f_iN,\vec{r}) = 1$, where $(i, j, k) \in \{(A, B, C), (B, C, A), (C, A, B)\}$.

Therefore, the local segment density of each block component can be obtained:

$$\phi_A(\vec{r}) = \frac{V}{Q}\int_0^{f_A} q_A(s,\vec{r})\,q_A^+(s,\vec{r})\,ds \quad (11)$$

$$\phi_B(\vec{r}) = \frac{V}{Q}\int_0^{f_B} q_B(s,\vec{r})q_B^+(s,\vec{r})\,ds \quad (12)$$

$$\phi_C(\vec{r}) = \frac{V}{Q}\int_0^{f_C} q_C(s,\vec{r})\,q_C^+(s,\vec{r})\,ds \quad (13)$$

Equations 1−3, 5, and 11−13 form a closed set of self-consistent equations. The equations are numerically implemented with a combinatorial screening algorithm proposed by Drolet and Fredrickson.[34,35] At first, initial random fields ω_A, ω_B, and ω_C are given. Second, the two partition functions $q_i(s,\vec{r})$ and $q_i^+(s,\vec{r})$ are then evaluated by solving eqs 9 and 10 with the pseudospectral numerical method. Third, the density fields are obtained by

(34) Drolet, F.; Fredrickson, G. H. *Phys. Rev. Lett.* **1999**, *83*, 4317–4320.
(35) Drolet, F.; Fredrickson, G. H. *Macromolecules* **2001**, *34*, 5317–5324.

eqs 11−13. Finally, with the obtained segment density, the fields are updated by a combination of their old and new values according to eqs 1−3. With the new fields, the partition functions $q_i(s, \vec{r})$ and $q_i^+(s, \vec{r})$ are evaluated again to obtain the segment density. These steps are iterated until the required self-consistency is reached[34] in which the free energy converges and is minimized to a stable value and the change in value decreases to 10^{-6}, and then the phase pattern emerging in the appointed simulation box can be clearly identified.

The numerical simulations are conducted in 3D space with periodic boundary conditions in the x, y, and z directions both in the bulk and for the case of confinement. The system is confined between two hard walls separated by L_z lattice points. The contour length is discretized as 100 segments, namely, $\Delta s = 0.01$, and the grid size in 3D space is $\Delta x = \Delta y = \Delta z = 0.245R_g$ in this work. To minimize the influence of the simulation box size in the x and y directions, each minimization of the free energy is iterated with respect to a variety of reasonable sizes ($5R_g$−$8R_g$) in the x and y directions (L_x, L_y = 20, 22, 24, ..., 32). It needs to be noted that the free energy of the final stable phase that is obtained by changing the simulation box size in the x and y directions is the minimal value obtained by comparing the free energies of all saddle point solutions to the SCMFT equations for an appointed film thickness. Furthermore, each minimization of the free energy is repeated and run several times using different initial random guesses of the potential fields ω_A, ω_B, and ω_C to ensure that the equilibrium morphology can be obtained exactly. In this way, typical ordered morphologies and the phase diagram are obtained for the star triblock copolymer confined between two hard walls by systematically adjusting the value of the thickness of the film and the strength of the surface field for different cases of Flory−Huggins interaction parameters at each appointed situation.

3. Results and Discussion

The confined ABC star triblock copolymer film system is specified by five series of parameters: f_i, χ_{ij}, Λ_i, Δ, and N. In our simulation, we fix the degree of polymerization of each chain for star triblock copolymer $N = 100$; this chain length is suitable for a reasonable description of the complicated microphase structures. The calculation is carried out on a 3D $L_x \times L_y \times L_z$ lattice with periodic boundary conditions in the x and y directions. The z direction is normal to the film surfaces, and $L_z = \Delta$ denotes the thickness of a film for an ABC star triblock copolymer in a confined system. To simplify the calculation, we assume that the properties of two substrates are symmetric, namely, $\Lambda = \Lambda_1 = \Lambda_2$. $\Lambda > 0$ indicates an attractive effect for segment A towards the substrate but a repellent effect for segments B and C. On the contrary, $\Lambda < 0$ indicates a repellent effect for segment A but an attractive effect for segments B and C in the star polymer. To simplify the calculation again, we choose nearly symmetric conditions of $f_A = f_B = 0.3$ and $f_C = 0.4$ to focus on the strong topological constraint of the star polymer chain under the condition of the confined thin film between two hard walls. Herein, the parameters in this work are reduced to three main factors: $\chi_{ij}N$, Δ, and Λ. Subsequently, critical $\chi_{ij}N$ for symmetric interactions among the different components of the $A_{0.3}B_{0.3}C_{0.4}$ star triblock copolymers is evaluated. The result shows that blocks A and B are mixed but separated from the C blocks according to $19 < \chi_{ij}N < 20$ whereas the A, B, and C blocks are completely separated according to $\chi_{ij}N > 22$. Then, three different degrees of segregation for the star copolymers have been determined in this work: a relatively weak segregation regime, a moderate segregation regime, and a strong segregation regime are set as the symmetric Flory−Huggins parameters $\chi_{ij}N$ corresponding to 20, 35, and 50, respectively. The microphase structure is determined in this work for different series of Flory−Huggins interaction parameters $\chi N = (\chi_{AB}N, \chi_{AC}N, \chi_{BC}N)$. We first discuss a case with symmetric interaction parameters between three species of the star polymer as $\chi N = (35, 35, 35)$. To analyze the influence of the asymmetry effect, we also focus on the other two series of asymmetric interaction parameters between the different species and discuses the phase behavior of the star triblock copolymers. For this effect, we first investigate the conditions under which blocks A and B are more favorable than those for the AC and BC pairs with asymmetric Flory−Huggins parameters $\chi N = (20, 50, 50)$. We then further discuss more unfavorable interaction parameters between blocks A and B, such as $\chi N = (50, 20, 20)$.

3.1. Bulk Morphologies. To investigate further the transition of the microstructures induced by the surface wall, we examine the morphologies of the $A_{0.3}B_{0.3}C_{0.4}$ star triblock copolymers on the basis of the SCMFT simulation results according to three different series of Flory−Huggins parameters. The calculated self-assembly morphologies of the star triblock copolymers are shown in Figure 5. Three distinct colors (blue, green, and red) are assigned to the A, B, and C blocks, respectively. A three-component hexagonal honeycomb polygonal cylinder phase was obtained with a symmetric interaction parameter of $\chi N = (35, 35, 35)$ (Figure 5a), which is in agreement with the results from a previous report.[9] The emergence of the individual hexagonal domain is due to the microphase separation between highly incompatible polymer components with a symmetric interaction parameter. When the series of interaction parameters was transferred to an asymmetric one ($\chi N = (20, 50, 50)$), there were different changes and the microstructure of a hexagonal elliptical cylinder phase formed by the C block was observed in Figure 5b. The polygonal cylinders of components A and B are packed in a pentagonal array with hexagonal-like and tetragonal-like alternating domains both for the A and B blocks. It can be presumed that the domains are arranged in such a manner so as to lower the surface energies between component C and the other two components. By adjusting the interaction parameter to $\chi N = (50, 20, 20)$, as shown in Figure 5c, although the microstructure of the system also takes a three-component hexagonal cylinder phase as in Figure 5a, we find that the domains of components A, B, and C are elliptical; the interfaces are somewhat diffuse because of relatively weaker repulsive interactions between these two different components in the triblock copolymers.

In the bulk of $A_{0.3}B_{0.3}C_{0.4}$ star triblock copolymers for three appointed interaction parameters, as shown in Figure 5, there is a common factor: the C-rich cylinders always arrange in a hexagonal manner for these three cases. The equilibrium period length P_i (i = 1, 2, 3), which is the distance between the two closest centers (C-rich cylinder) in two closest three-component hexagonal cylinder units, is found to be $P_1 \approx 6.0R_g$ in Figure 5a, $P_2 \approx 7.5R_g$ in Figure 5b, and $P_3 \approx 6.5R_g$ in Figure 5c. The frustration of the polymer period would reorient the cylinders' direction in the self-assembled film in this work as pointed out by Wang in the case of planar confinement.[15] Thus, in this work, we order the self-assembled structures as a function of Δ/P_i (where Δ is the film thickness and P_i (i = 1, 2, 3) is the length of the equilibrium period for the C-rich cylinders in Figure 5a−c, respectively) to describe the degree of confinement and the orientation transformation for self-assembled films of star triblock copolymers.

3.2. Phase Behavior of a Thin Film. In our simulation, by considering the range of film thickness and block−substrate interactions at symmetric and asymmetric interaction parameters

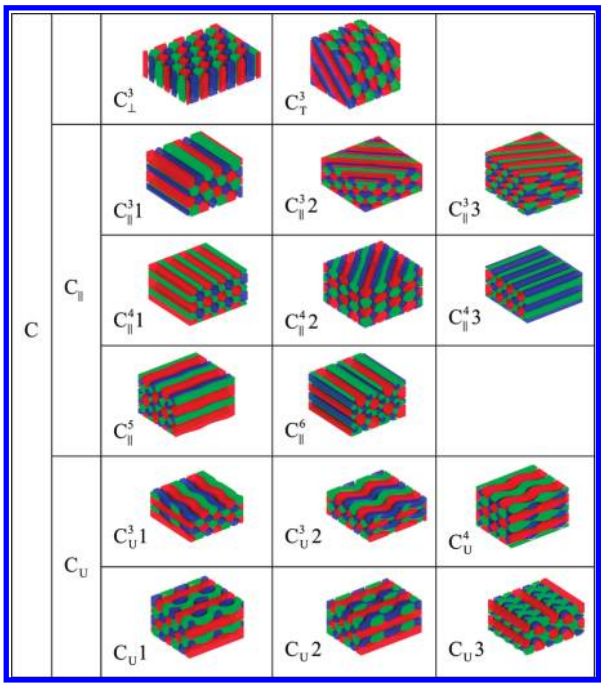

Figure 1. Cylindrical structures of thin films under confinement. The blue, green, and red regions represent isodensity surface distributions of the A, B, and C blocks in the $A_{0.3}B_{0.3}C_{0.4}$ star triblock copolymer, respectively.

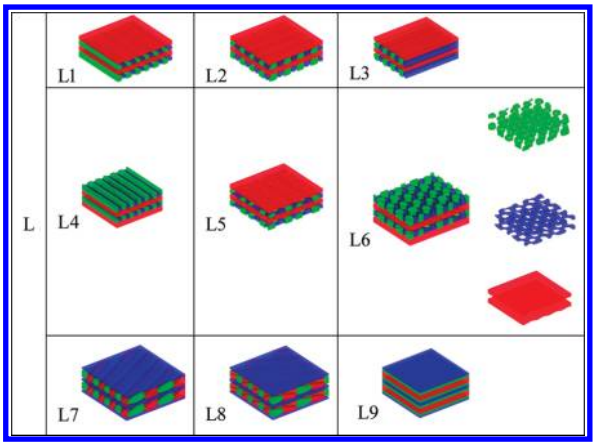

Figure 2. Lamellar structures of thin films under confinement. The blue, green, and red regions represent isodensity surface distributions of the A, B, and C blocks in the $A_{0.3}B_{0.3}C_{0.4}$ star triblock copolymer, respectively.

between different block species in the $A_{0.3}B_{0.3}C_{0.4}$ star triblock copolymer, we identify different microphases found in the simulation by a visual assessment of the density profile, including a series of complex microphases such as cylinders, undulating cylinders, lamellae, perforated lamellae, and hybrid network structures to facilitate the comparison of structures with different surface properties. For the different type of parameters that we have explored, these morphologies can be divided into four primary classes: (1) cylinders, (2) lamellae, (3) perforated lamellae, and (4) complex hybrid structures. Meanwhile, each morphology class contains several kinds of related structures. The structures are shown in Figures 1−4.

3.2.1. Cylinders (*C*). Although cylinders are the bulk phase, they are not always dominant in thin films of star triblock copolymers. There are four kinds of cylinders found in our screening, as shown in Figure 1:

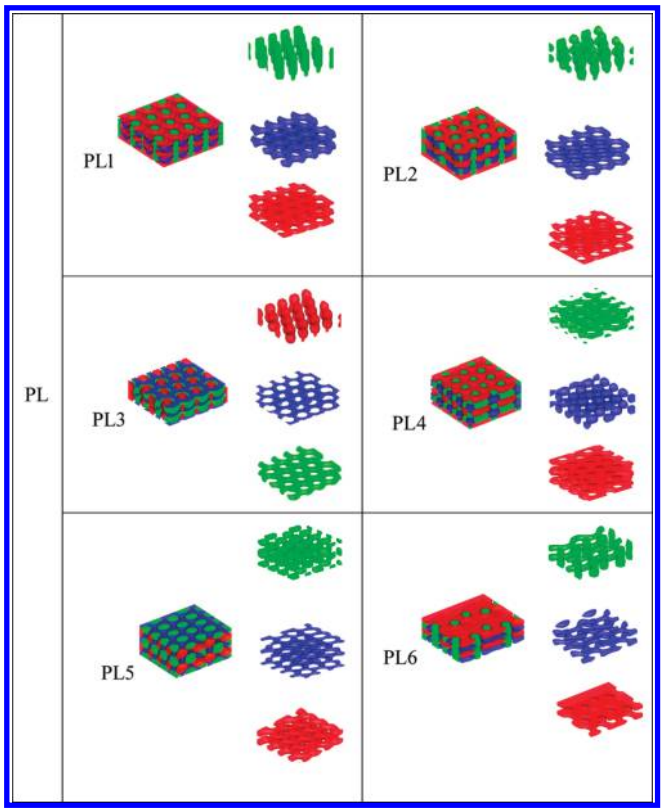

Figure 3. Perforated lamellae of thin films under confinement. The blue, green, and red regions represent isodensity surface distributions of the A, B, and C blocks in the $A_{0.3}B_{0.3}C_{0.4}$ star triblock copolymer, respectively.

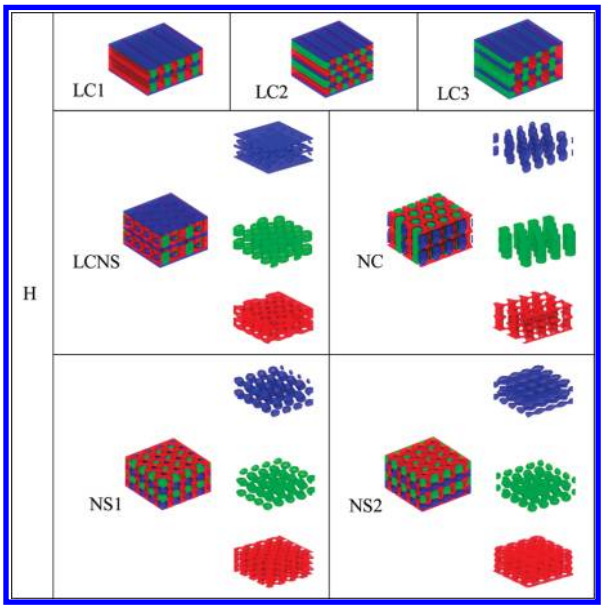

Figure 4. Hybrid structures of a thin film under confinement. The blue, green, and red regions represent isodensity surface distributions of the A, B, and C blocks in the $A_{0.3}B_{0.3}C_{0.4}$ star triblock copolymer, respectively.

Perpendicular Cylinders ($C_{\perp}^{3}$). In this case, the cylinders are aligned perpendicular to the substrates, and the three-component cylinders are arranged in a hexagonal lattice.

Tilted Cylinders (C_{T}^{3}). tilted three-component hexagonal cylinders.

Parallel Cylinders ($C_{\parallel}$). The cylinders are parallel to the substrates. We have $C_{\parallel}^{3}$, $C_{\parallel}^{4}$, $C_{\parallel}^{5}$, and $C_{\parallel}^{6}$. The number in the upper

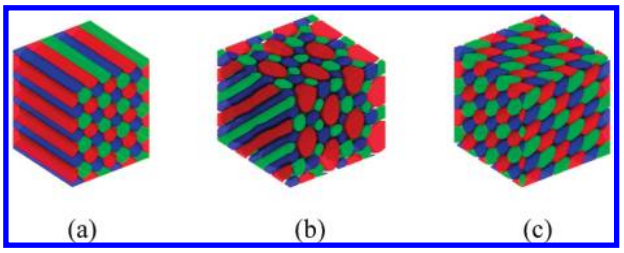

Figure 5. Equilibrium morphologies for $A_{0.3}B_{0.3}C_{0.4}$ star triblock copolymers in the bulk. The blue, green, and red regions represent the density distributions of the monomers belonging to A, B, and C blocks, respectively. The interaction parameters between the components are (a) $\chi N = (35, 35, 35)$, (b) $\chi N = (20, 50, 50)$, and (c) $\chi N = (50, 20, 20)$.

right corner denotes the number of cylinders of block A or block B surrounding the center of block C in the thin film counted in the z direction. The number 1−3 in morphologies $C_{\parallel}^{3}1-C_{\parallel}^{3}3$ and $C_{\parallel}^{4}1-C_{\parallel}^{4}3$ denotes the different orientation angles of the parallel cylinders ($C_{\parallel}^{3}$, $C_{\parallel}^{4}$) in the appointed xz plane (or yz plane).

It is interesting that all of the polygonal structures that we obtained ($C_{\perp}^{3}$, C_{T}^{3}, $C_{\parallel}$ agree well with the results of Monte Carlo simulations by Gemma[29] and bulk morphologies of ABC linear and ABC star triblock copolymers studied by Qiu.[9,36] Actually, $C_{\parallel}^{3}$ (including $C_{\perp}^{3}$ and C_{T}^{3}), $C_{\parallel}^{4}$, and $C_{\parallel}^{5}$ were reported to be a three-color hexagonal honeycomb phase (HEX3), an octagon−octagon−tetragon phase (OOT), and a decagon−hexagon−tetragon phase (DEHT) in 2D space.[9,36]

Undulating Cylinders (C_U). There are two different types: One type consists of cylinders that are not straight but undulate between two surfaces and the peaks of neighboring cylinders are interlaced (C_{U}^{3} and C_{U}^{4}). However, a cylinder of block C is straight in the other type of undulating cylinders in which they are subdivided into C_U1, in which block B was an undulating cylinder and block A was dispersed as beads, C_U2, in which block A was an undulating cylinder and block B was dispersed as beads, and C_U3, in which blocks A and B had an array of interlaced dumbbells. The number 1 or 2 in morphology $C_{U}^{3}1$ or $C_{U}^{3}2$ denotes the different orientation angle of the undulating cylinders (C_{U}^{3}) in the appointed xz plane (or yz plane).

3.2.2. Lamellae (L). If the surface interaction energy between the blocks in the star triblock copolymer and substrates dominates, then the lamellae structure could be more favorable than cylinders. There are three kinds of lamellae parallel to substrates shown in Figure 2.

Flat Lamellae for Block C ($L_C + L_{AB}$). In this case, L1−L4 are the lamellae structures in which a lamellar layer of block C is parallel to the substrates (L_C), although blocks A and B separate not as cylinders but as a lamellar array as a whole (L_{AB}). The number between 1 and 3 on the right side of morphologies L1−L3 denotes the different orientation angle of the lamellar layer L_{AB} in the appointed xz plane (or yz plane). However, the number of 4 in L4 denotes a mirror image morphology (along the z direction) of L1.

Although L5 and L6 are the lamellae structures in block C as a lamellar layer (L_C), blocks A and B are secondary perforated lamellae (L_{AB} stands for L_{PLAB}). There are a couple of mirror image morphologies along the z direction as well.

Flat Lamellae for Block A ($L_A + L_{BC}$). Lamellae structures L7 and L8 are the block A lamellar layer (L_A), and blocks B and C are separated as cylinders and as a lamellar layer as a whole (L_{BC}). The number 7 or 8 in morphology L7 or L8 denotes the different orientation angle of the lamellar layer L_{BC} in the appointed xz plane (or yz plane).

Flat Lamellae for Three Blocks A, B, and C ($L_A + L_B + L_C$ = LAM3). L9 is a lamellar structure in which each block constitutes an individual layer, namely, LAM3, as reported in other works.[9,36]

3.2.3. Perforated Lamellae (PL). The perforated lamellae structure is a metastable microphase in the bulk phase of diblock copolymers and linear triblock copolymers as proven by strong segregation theory and SCMFT. However, it is stable under thin film conditions for the star triblock copolymer as a result of the confinement and preference of the substrates, although the perforated lamellae found in the melt of the star copolymer is not a truly stable structure as reported by Gemma.[29] The perforated lamellae are also parallel to the substrates, and in most situations, the pores are arranged in a hexagonal lattice as shown in Figure 3. PL1 contains two individual perforated lamellar layer for blocks A and C with intermediary cylinders of block B packaged in the pores. PL2 contains two perforated lamellar layers as PL1 with altering cylinders and beads of block B packaged in the pores in the perforated lamellar layer. PL3 contains a perforated lamellar layer for blocks A and B with intermediary cylinders of block B packaged in the pores. PL4 contains two perforated lamellar layers for blocks B and C, and there is a layer of disperse beads of block B located above the pores in each lamellar layer of block B, which is packaged in the pores in the lamellar layer of block C. Meanwhile, the disperse beads of block A are packaged in the pores of perforated lamellar block B. PL5 contains a single perforated lamellar layer for block C with disperse beads of block A packaged in its pores whereas block B in PL5 is dispersed as beads and is packaged in the pores of block A. PL6 consists of blocks A and C acting as a perforated lamellar layer with perpendicular and undulating parallel cylinders of block B packaged in the perforated lamellar layer.

3.2.4. Complex Hybrid Structures (H). We have also found stable hybrid structures of lamellae (L), cylinders (C), spheres (S), and a network (N). We use two or more letters to denote the types of mixture as shown in Figure 4. For example, LC means a mixed structure of lamellae and cylinders.

A-Rich Wetting Layers. LC1 contains C-rich dumbbell cylinders in the middle of the structure and A- and B-rich slightly flat cylinders complementary to the dumbbell cylinder with two flat A-rich wetting layers. LC2 contains C-rich cylinders in the middle of the structure and a hexagonal array for A- and B-rich cylinders with two flat A-rich wetting layers. LC3 contains C-rich slightly flat cylinders in the middle of the structure, and the A- and B-rich parallel cylinders together act as a crossed structure with two flat A-rich wetting layers. LCNS contains B-rich short cylinders perpendicular to the substrates, and most of block A is dispersed as small spheres with two A-rich wetting layers and a network structure of block C.

C-Rich Perforative Network Structure. NC consists of A-rich short cylinders and B-rich cylinders that when perpendicular to the substrates together act as fillers for the C-rich network structure. NS1 contains blocks A and B dispersed alternately as regular cubic spheres, analogous to a typical CsCl structure, and packaged in the pores of the C-rich perforative network structure. By comparison with the critical value of the sum of the fractions of the A and B components in which the spheres of NS1 are dispersed with same radii, we find that the spheres between blocks A and B are different in size in this work, so the sum of the fractions of the A and B components might be less than the critical volume fraction. However, even though the sum of the fractions for the A and B components is 0.6 in this work, which deviates from the theoretical critical value of 0.68 reported

(36) Tang, P.; Qiu, F.; Zhang, H. D.; Yang, Y. L. *Phys. Rev. E* **2004**, *69*, 031803.

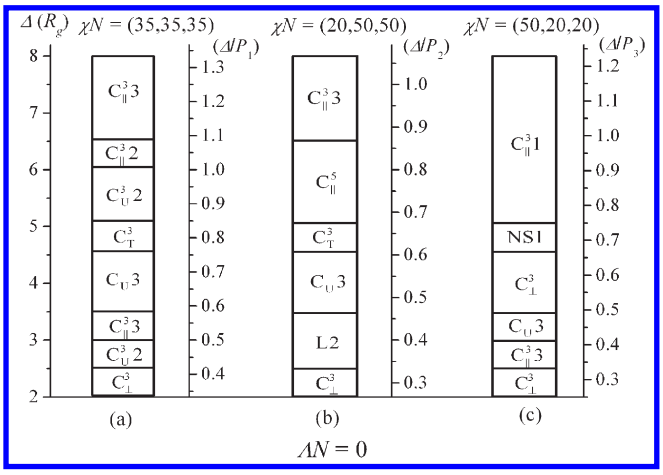

Figure 6. Phase diagrams of $A_{0.3}B_{0.3}C_{0.4}$ star triblock copolymer thin films confined inside neutral walls ($\Lambda N = 0$) as a function of film thickness for symmetric and asymmetric interactions between different polymer species: (a) $\chi N = (35, 35, 35)$, (b) $\chi N = (20, 50, 50)$, and (c) $\chi N = (50, 20, 20)$. Squares indicate the range of each kind of morphology as shown in Figures 1−4.

by Hayashida et al.,[37] NS1 still appears in Figures 8c, 10c, 13c, and 14c (including Figure 6c), which might be attributed to the appointed strength of the surface field that has been implemented in each of these cases. Nevertheless, the upper surface of NS1 has a structure with 3-fold symmetry. NS2 contains block B dispersed as regular spheres and block A disperses as elongated spheres and connected so as to form consecutive shuttles with a C-rich network structure.

The phase behavior of the thin film under confinement, as shown in Figures 1−4, is a summary profile for the morphology in each simulation. For consistency, we display the morphology with two repeats units in Figures 1−4. If the time of the morphology repeat is given as one time, then some of the morphology of the confined film would not be as clear as the morphology in Figures 1−4. When three or more integral repeat units of morphology are adopted, the morphology can also be divided into identical and individual parts in two repeat time units, which seems to refer to the structure of a crystal; a clear distinction of the morphology of a cell needs to be given. However, on the basis of the different repeat lengths of the bulk for the $A_{0.3}B_{0.3}C_{0.4}$ star triblock copolymer, according to the different series of interaction parameters, $P_1 \approx 6.0R_g$ for $\chi N = (35, 35, 35)$, $P_2 \approx 7.5R_g$ for $\chi N = (20, 50, 50)$, and $P_3 \approx 6.5R_g$ for $\chi N = (50, 20, 20)$. The more detailed repeat times of morphology in each simulation can be evaluated by the Δ/P_i ($i = 1, 2, 3$) repeat parameter, which includes integral and nonintegral times, shown as the vertical axes in Figures 6−10.

The influence of the molecular architecture on the observed microstructures can be clearly distinguished by comparing our results with the behavior of ABC linear and star triblock copolymers under confinement.[23,25] These structures, such as the perpendicular, tilted, and parallel cylinders, flat lamellae, and perforated lamellae, have been observed in previous simulation and experiment works.[4,8,21,27,38−48] However, to our knowledge, it is significant for the star triblock copolymer that some new structures such as the undulating cylinder and hybrid structure mixed network and spheres are found and, as mentioned above, are also proven to be stable by comparing their free energy with that of other structures at the appointed strength of the surface field and film thickness. Simulation parameters such as the Flory−Huggins interaction parameter (χN), field strength of the substrates (ΛN), and thickness of the film (Δ) are similar in the above studies, which facilitates comparison.

3.3. For Neutral Walls. The transformation among the different morphologies is the result of frustration effects by confinement and surface fields in polymer self-assembly processes of thin films. To distinguish among them, we first consider the effect of confinement alone in which ABC star triblock copolymers are confined between two parallel neutral substrates without any preferential attraction for either polymer species ($\Lambda N = 0$). The phase behavior is investigated by systematically varying the film thickness with symmetric interaction parameter $\chi N = (35, 35, 35)$ as well as with asymmetric interaction parameters $\chi N = (20, 50, 50)$ and $(50, 20, 20)$. The phase diagrams according to different interaction parameters under the condition of neutral substrates is shown as Figure 6. The vertical axes of these diagrams (Figures 6−10) denote the thickness of the film in units of R_g for each appointed interaction. An obvious change in phase behavior with confined substrates contrasting with the microphase is observed for different interactions in the bulk (cylinders).[8]

In Figure 6, even for different degrees of segregation for polymer species in the star triblock copolymer, the perpendicular cylinder ($C_{\perp}^3$) was obtained in the thin film ($\Delta < 2.5R_g$) when the repeat parameters are $\Delta/P_1 < 0.42$ for Figure 6a, $\Delta/P_2 < 0.33$ for Figure 6b, and $\Delta/P_3 < 0.38$ for Figure 6c in this work; we conclude that $C_{\perp}^3$ arises only in small repeat parameter Δ/P_i ($i = 1, 2, 3$). The results of ordered cylindrical morphology in confined thin films of diblock and linear triblock copolymers showed that the perpendicular morphology existed in a discontinuous range of film thickness and with increasing film thickness; the range decreases and the perpendicular morphology cannot be observed in thick films.[49] MC simulation results of linear triblock copolymer system under confinement also showed that the thickness range of perpendicular cylinders decreased more quickly than that in diblock copolymer systems.[26]

The microphase with three-component cylinders arranged in a hexagonal lattice and aligned parallel to the substrates, $C_{\parallel}^3$ ($C_{\parallel}^3 1$, $C_{\parallel}^3 3$), have been observed in the following ranges of repeat parameters: $\Delta/P_1 > 1.0$, $\Delta/P_2 > 0.87$, and $\Delta/P_3 > 0.76$. These correspond to different interaction parameters $\chi N = (35, 35, 35)$ (Figure 6a), $\chi N = (20, 50, 50)$ (Figure 6b), and $\chi N = (50, 20, 20)$ (Figure 6c), respectively. However, with increasing film thickness, they both demonstrate an analogous morphology of the

(37) Hayashida, K.; Takano, A.; Dotera, T.; Matsushita, Y. *Macromolecules* **2008**, *41*, 6269–6271.
(38) Harrison, C.; Park, M.; Chaikin, P.; Register, R. A.; Adamson, D. H.; Yao, N. *Polymer* **1998**, *38*, 2733–2744.
(39) Thurn-Albrecht, T.; Steiner, R.; DeRouchey, J.; Stafford, C. M.; Huang, E.; Bal, M.; Tuominen, M.; Hawker, C. J.; Russell, T. P. *Adv. Mater.* **2000**, *12*, 787–791.
(40) Lammertink, R. G. H.; Hempenius, M. A.; Vancso, G. J. *Langmuir* **2000**, *16*, 6245–6252.
(41) Yokoyama, H.; Mates, T. E.; Kramer, E. J. *Macromolecules* **2000**, *33*, 1888–1898.
(42) Fasolka, M. J.; Banerjee, P.; Mayes, A. M.; Pickett, G.; Balazs, A. C. *Macromolecules* **2000**, *33*, 5702–5712.
(43) Lammertink, R. G. H; Hempenius, M. A.; Vancso, G. J.; Shin, K.; Rafailovich, M. H.; Sokolov, J. *Macromolecules* **2001**, *34*, 942–950.
(44) Segalman, R. A.; Hexemer, A.; Kramer, E. J. *Macromolecules* **2003**, *36*, 6831–6839.
(45) Knoll, A.; Horvat, A.; Lyakhova, K. S.; Krausch, G.; Sevink, G. J. A.; Zvelindovsky, A. V.; Magerle, R. *Phys. Rev. Lett.* **2002**, *89*, 035501.
(46) Sevink, G. J. A.; Fraaije, J. G. E. M.; Huinink, H. P. *Macromolecules* **2002**, *35*, 1848–1859.
(47) Lyakhova, K. S.; Sevink, G. J. A.; Zvelindovsky, A. V.; Horvat, A.; Magerle, R. *J. Chem. Phys.* **2004**, *120*, 1127–37.
(48) Knoll, A.; Lyakhova, K. S.; Horvat, A.; Krausch, G.; Sevink, G. J. A.; Zvelindovsky, A. V.; Magerle, R. *Nat. Mater.* **2004**, *3*, 886–890.
(49) Suh, K. Y.; Kim, Y. S.; Lee, H. H. *J. Chem. Phys.* **1998**, *108*, 1253–1256.

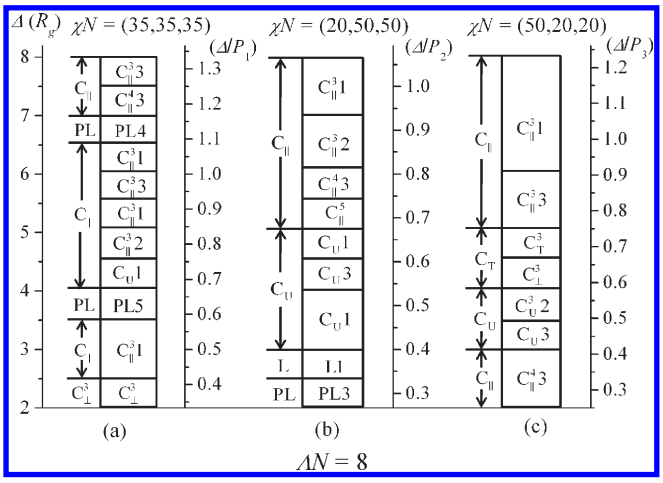

Figure 7. Phase diagrams of $A_{0.3}B_{0.3}C_{0.4}$ star triblock copolymer thin films confined inside weak preferential walls ($\Lambda N = 8$) for symmetric and asymmetric interactions between different polymer species: (a) $\chi N = (35, 35, 35)$, (b) $\chi N = (20, 50, 50)$, (c) $\chi N = (50, 20, 20)$. Squares indicate the range of each kind of morphology as shown in Figures 1−4.

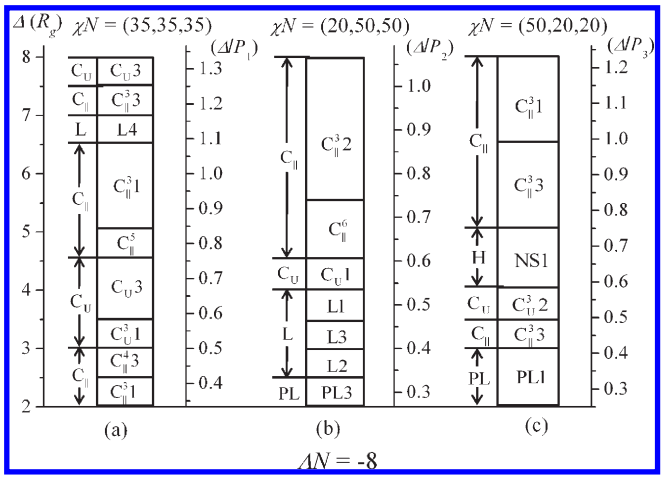

Figure 8. Phase diagrams of $A_{0.3}B_{0.3}C_{0.4}$ star triblock copolymer thin films confined inside weak preferential walls ($\Lambda N = -8$) as a function of film thickness for symmetric and asymmetric interactions between different polymer species: (a) $\chi N = (35, 35, 35)$, (b) $\chi N = (20, 50, 50)$, and (c) $\chi N = (50, 20, 20)$. Squares indicate the range of each kind of morphology as shown in Figures 1−4.

cylindrical structure as a whole. They are alternating undulating and nonundulating cylinder structures as well. This phenomenon is prominently displayed in Figure 6a, where the change in the microphase is $C_{\perp}^3-C_U^3-C_{\parallel}^3-C_U3-C_T^3-C_U^3-C_{\parallel}^3$. Similarly, undulating cylinders had been explored for diblock copolymer thin films under a symmetric surface field and both the ABA linear and ABC star triblock copolymer thin films have been explored under an asymmetric surface field. Nevertheless, C_U undulating cylinder structures occur in this work for both neutral substrates (Figure 6) and preferential substrates (Figures 7, 8, and 10). There are two main reasons for this: One is that the contorted structure can effectively adapt to the repeat parameter to minimize unfavorable contacts with other components and substrates. The other is the entropic effect from the limitation of the junction point in the star triblock copolymer. Both of them induce the appearance of the undulating cylinders.

Although PL morphology was widely found both in diblock copolymer thin films and ABC linear triblock copolymer thin films, whereas in this work the PL structure did not occur for the neutral substrates, which agrees well with the results from Chen and Ludwigs, they reported that the PL structure occurred only for a confined system with a surface field added.[24,27] We conclude that the driving force for the constraint of the star point is insufficient to control the formation of the PL phase for an ABC star triblock copolymer without a surface field. Furthermore, we note that in the PL structures B-rich perforated lamellae cannot occur at the surfaces. Because the composition of different species for $A_{0.3}B_{0.3}C_{0.4}$ is almost symmetrical, the attraction for block B is very small from the entropic preference effect and cannot manipulate the formation of perforated lamellae near the surface. From Figure 6b, we can see a larger region of parallel cylinders than that which emerges under a weak preference (Figure 7a) because of the strong incompatibility between components C and A (B). The C-rich lamellae are adjusted to match A-rich and B-rich cylinders under the constraint of the star junction point shown as L2 in Figure 6b as a result of the relatively weaker interaction between blocks A and B ($\chi_{AB}N = 20$). Although an NS1 structure emerges in the range of $0.76 > \Delta/P_3 > 0.69$ for the interaction parameter $\chi N = (50, 20, 20)$ (Figure 6c), it may due to the coupling effects of confinement and star architecture.

3.4. Preferential Walls. *3.4.1. Weak Substrate Preference.* In the following text, we use a combined parameter ΛN to denote the interaction between a substrate and block. We choose $\Lambda N = \pm 8$ for the weak substrate preference case because ΛN is the difference between the block−substrate interactions. The absolute ratio of $|\Lambda N/\chi_{ij}|$ is a good way to illustrate the relative strength of the substrate selectivity. In Figures 7 and 8, $|\Lambda N/\chi_{ij}|$ ranged between 0.16 and 0.4, corresponding to a fairly weak interaction between the blocks and substrates. A reversed surface preference leads to two completely different phase diagrams because the star triblock copolymer itself (volume composition) is not absolutely symmetric.

There is a little difference between Figures 7 and 8; however, the cylinder phase dominates almost the entire range of film thickness. The most important factor that affects the phase diagram of the confined cylindrical block copolymers may be the preference of the two surfaces of the substrates. When the surface attraction is not strong enough to overpower the entropic energy needed to create a wetting layer of one species, the system will be composed of cylinders ($C_{\perp}$, $C_{\parallel}$, or C_U) with a slight deformation near each surface. The thermodynamically stable L and P phases are also found in certain film thickness in Figures 7 and 8, but they completely disappear in Figure 7c. We also find that contorted lamellae phases (L1, L2, L3) appear near the boundary of the flat lamellae regions. The waves in the undulating lamellae are usually too obscure to differentiate from the regular flat lamellae in this work. We are not able, in the present stage, to determine which pattern is more stable because the existence of these structures depends on the simulation box size and their free energies are too similar, beyond the precision of the calculation. However, we are sure that the lamellae structures are thermodynamically stable because the free energies of both the undulating lamellae and the regular flat lamellae are lower than those of any other structures. To match the film thickness under confinement, the flat surfaces of the regular lamellae have to be distorted into undulating surfaces with external strain.

We now discuss the complex hybrid structure mixing of more than two different pure and individual structures. We note that in Figures 6 and 8 there are regions where the hybrid structures (e.g., NS1) are stable. Typical types of these hybrid structures are shown in Figure 4. Usually, at a particular point in the H region,

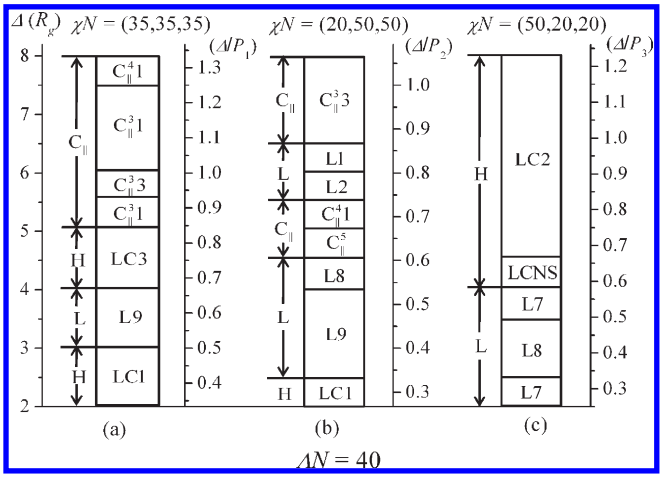

Figure 9. Phase diagrams of $A_{0.3}B_{0.3}C_{0.4}$ star triblock copolymer thin films confined inside strong preferential walls ($\Lambda N = 40$) as a function of film thickness for symmetric and asymmetric interactions between different polymer species: (a) $\chi N = (35, 35, 35)$, (b) $\chi N = (20, 50, 50)$, and (c) $\chi N = (50, 20, 20)$. Squares indicate the range of each kind of morphology as shown in Figures 1−4.

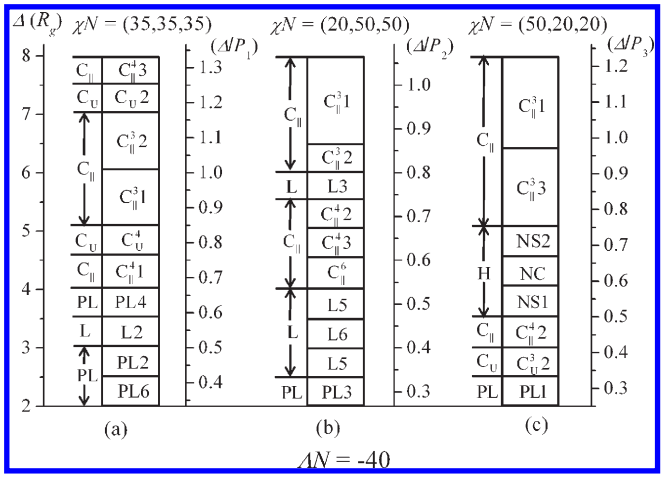

Figure 10. Phase diagrams of $A_{0.3}B_{0.3}C_{0.4}$ star triblock copolymer thin films confined inside strong preferential walls ($\Lambda N = -40$) as a function of film thickness for symmetric and asymmetric interactions between different polymer species: (a) $\chi N = (35, 35, 35)$, (b) $\chi N = (20, 50, 50)$, and (c) $\chi N = (50, 20, 20)$. Squares indicate the range of each kind of morphology as shown in Figures 1−4.

there can be several types of hybrid structures; each has a free energy lower than that of any other pure structures.[4] There are too many possible combinations of these structures, and the free-energy differences among these mixed phases sometimes are small, as reported with the alternative direction implicit method (ADI);[4] however, we can clearly identify which one is the most stable by using a pseudospectral numerical method due to higher-precision contrasting ADI in the simulations when searching the morphologies. Therefore, we draw a detailed structure of the H region in Figures 6 and 8, in which the simulation results shown as Figure 4 include LC, NC, NS, and LCNS hybrid structures.

3.4.2. Strong Substrate Preference. To study the effect of a surface field on the microstructure of confined ABC star triblock copolymers as a function of film thickness when the appointed preferential effect was added, we sample for two different situations corresponding to attractive ($\Lambda N > 0$) and repulsive ($\Lambda N < 0$) surfaces for block A. Phase diagrams for $A_{0.3}B_{0.3}C_{0.4}$ star triblock copolymer thin films confined with a strong preferential attraction for block A ($\Lambda N = 40$) are shown in Figure 9. With increasing film thickness, the sequence of microphase transformation is H−L−H−$C_{\parallel}$, H−L−$C_{\parallel}$−L−$C_{\parallel}$, and L−H for $\chi N = (35, 35, 35)$ (Figure 9a), $\chi N = (20, 50, 50)$ (Figure 9b), and $\chi N = (50, 20, 20)$ (Figure 9c), respectively. We observe that there is a little different tendency toward the transition of microstructures with the increase in film thickness by examining a thin film confined with neutral surfaces (Figure 6). Although the analogous $C_{\parallel}$ microphases arise in the larger repeat parameters, $\Delta/P_1 > 0.83$ and $\Delta/P_2 > 0.87$ for the symmetric interaction of $\chi N = (35, 35, 35)$ (Figure 9a) and the asymmetric interaction of $\chi N = (20, 50, 50)$ (Figure 9b), respectively, in this work, there are predominant lamellae and hybrid structures displayed under the strong attractive walls. Meanwhile, there is a visible phenomenon that the lamellae layer structures (LC1−LC3, L1−L2, L7−L9) in equilibrium morphologies with the surface field seem to replace the cylinder structures under the same conditions of neutral walls. We also find that in the equilibrium morphologies (LC1−LC3, L7−L9) block A was attracted by the substrates and formed as a wetting layer at the surface because of a strong effective attraction from the walls despite the strong segregation between blocks A and B in Figure 9c. In Figure 9c, even though there are weak segregations between blocks C and A (B), the three-component hexagonal cylinder structure still appears between two wetting layer of block A, resulting from an incidental repellent effect for blocks A and B from the added surface field in very thick films and from a large range of repeat parameter $\Delta/P_3 > 0.69$. This intriguing finding reveals that the confinement and surface field can affect the degree of microphase separation and the morphology transformation in the confined film.

Figure 10 shows the transformation of microstructures as a function of film thickness when the walls have an effective repellency on block A with a appointed strength of the surface field of $\Lambda N = -40$. We observe the following structures as the film thickness increases: PL−L−PL−$C_{\parallel}$−C_U−$C_{\parallel}$−C_U−$C_{\parallel}$, PL−L−$C_{\parallel}$−L−$C_{\parallel}$, and PL−C_U−$C_{\parallel}$−H−$C_{\parallel}$. The cylindrical film has a larger repeat parameter range (there is a larger thickness range for the cylinder film): $\Delta/P_1 > 0.67$, $\Delta/P_2 > 0.53$, and $\Delta/P_3 > 0.76$ for $\chi N = (35, 35, 35)$ (Figure 10a), $\chi N = (20, 50, 50)$ (Figure 10b), and $\chi N = (50, 20, 20)$ (Figure 10c), respectively, especially for the parallel cylinder phases. There is also an interesting phenomenon in a large film thickness range in Figure 10a in which the parallel and undulating cylinder structures alternately emerge with an oscillating morphology transformation. We conclude that for this case of strong preferential repellent walls ($|\Lambda N/\chi_{ij}| = 1.14$), the block−substrate interaction is nearly equivalent to the Flory−Huggins interaction parameter of the star polymer. In other words, this substrate selectivity was not a dominant factor in controlling the morphology of the film. The cylinder phase is prevalent over a wide range of film thickness because of the radius of blocks in the ABC star copolymer and the shapes of the thin films can be flexibly manipulated by the star junction point constraint in order to accommodate different film thicknesses. Similar results had been obtained with confined ABA and ABC linear copolymers systems.[21,27]

The PL structure (PL1−PL4, PL6) occurred only in a thinner polymer film confined with a repellent surface field added in this case because the driving force from the constraint of the star point can adaptively control the appearance of the PL phase for ABC star triblock copolymers. In Figures 9 and 10, we find that the lamellae structure with cylinders ($L_C + L_{AB}$, L1−L3) occurs in relatively thick films in contrast to the case of neutral walls. In fact, the domain spacing of the lamellae with the cylinder

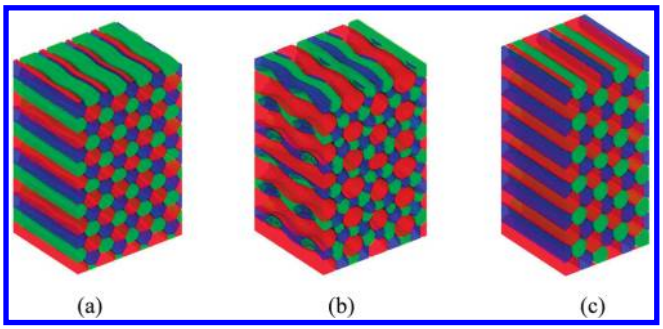

Figure 11. Equilibrium morphologies of thicker films ($\Delta = 12R_g$) for $A_{0.3}B_{0.3}C_{0.4}$ star triblock copolymers confined with a weaker substrate preference: (a) $\Lambda N = 4$, (b) $\Lambda N = 12$, and (c) $\Lambda N = 0$. The interaction parameters between the components are (a) $\chi N = (35, 35, 35)$, (b) $\chi N = (20, 50, 50)$, and (c) $\chi N = (50, 20, 20)$. The blue, green, and red regions represent the density distributions of the monomers belonging to A, B, and C blocks, respectively.

structure is relatively small compared to the bulk structure and the effect of the star junction point on the structure becomes less important, which implies that the surface interaction energy between polymer blocks and substrates dominantly controls the emergence of this structure.

3.5. Thicker Film Coupled with a Weaker Substrate Preference. To investigate the film thickness of the star triblock copolymer becoming larger and larger and how to affect its morphologies under surface confinement, we choose to study thicker films of $\Delta = 12R_g$ as shown in Figure 11. We find that in the relatively thicker films coupled with a weak substrate preference, in which the effect of the surface field becomes less important, cylindrical structures occur in the center of the film over a large range of film thickness, which is the same as the case for the bulk phase shown in Figure 5. However, something subtle arises in these cylindrical structures: the domain spacing is relatively small in contrast to the bulk structures and the effect of the star junction point on the structure is weakened when the distance between the two confined walls becomes larger, thus leading to some transitional morphology such as a multiple undulating cylindrical morphology that mixes with the structures of C_U^4 and C_U^5 as shown in Figure 11b. These transitional forms also demonstrate that the morphology in each simulation would approach that of the bulk phase (Figure 5) as long as the film thickness is large enough (e.g., $\Delta \geq 12R_g$), which can decrease the strength of the surface field. We just have exerted a limited strength of the surface field on the top and the bottom of the star polymer films for typical examples in Figure 11. As expected, even for $\Delta \geq 12R_g$, when the strength of the surface field is great enough to adapt to the effect of the film thickness, the morphology in each simulation should be the same as shown in Figures 1−4 under surface confinement.

3.6. Influence of the Strength of the Surface Field. A cylindrical phase in thin films of star triblock copolymers goes through a transition (C−L) and finally transforms into a lamellae structure between selective surfaces. This C−L transition in thin films has been predicted by different theories[14,15,50] and observed in various experiments.[38,51−53]

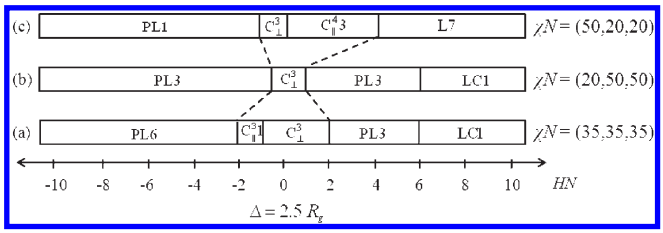

Figure 12. Morphology stability regions for $A_{0.3}B_{0.3}C_{0.4}$ star triblock copolymer thin films as a function of the surface field (HN) at $\Delta = 2.5R_g$ for different series of interaction parameters among components (a) $\chi N = (35, 35, 35)$, (b) $\chi N = (20, 50, 50)$, and (c) $\chi N = (50, 20, 20)$. Squares indicate the range of each kind of morphology as shown in Figures 1−4. The dashed lines indicate the structural transition between the cylindrical and noncylindrical phases.

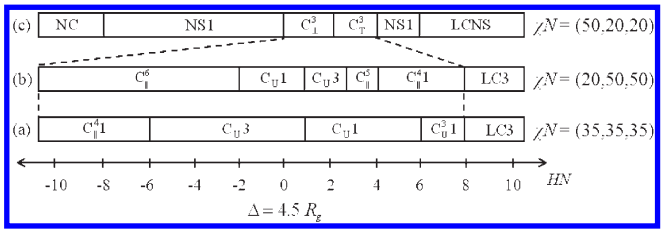

Figure 13. Morphology stability regions for $A_{0.3}B_{0.3}C_{0.4}$ star triblock copolymer thin films as a function of the surface field (HN) at $\Delta = 4.5R_g$ for different series of interaction parameters among components (a) $\chi N = (35, 35, 35)$, (b) $\chi N = (20, 50, 50)$, and (c) $\chi N = (50, 20, 20)$. Squares indicate the range of each kind of morphology as shown in Figures 1−4. The dashed lines indicate the structural transition between cylindrical and noncylindrical phases.

In this section, we will investigate how the transition of the film phase behavior is influenced by the strength of the surface field. For the sake of clarity, we give our full consideration to the strength of the surface field ($H(\vec{r})N_{0\leq z\leq \varepsilon} = H(\vec{r})N_{\Delta-\varepsilon\leq z\leq \Delta} = {}^1/_4\Lambda N = HN$) spanning the range between strongly repulsive ($HN = -10.5$) and strongly attractive surfaces ($HN = 10.5$) for the A block in an ABC star triblock copolymer under confinement.

To study the coupling effects of confinement and the surface field, it is significant to present the effect of the surface field for a relatively thinner film ($\Delta = 2.5R_g$). Figure 12 illuminates the phase diagrams of polymer films under different surface field strengths on an appointed thinner film. The $C_\perp$ phase is found in the lower absolute surface strength, and its value is not more than 2 ($|HN| \leq 2$) for three different series of interaction parameters. It reveals to us that, in most situations, the appearance of the $C_\perp$ phase in thinner films is due to the weak substrates' preference but is not exclusively determined by the thickness of the film. Figure 13 also shows that the $C_\perp$ phase can be found in thicker films ($\Delta = 4.5R_g$) with a weak preference. These results are in good agreement with the polymer films under confinement with neutral walls (Figure 6). As the absolute strength of the surface field ($|HN|$) for the A component increases, the $C_\parallel$ phase ($C_\parallel^3 1$ in Figure 12a, $C_\parallel^4 3$ in Figure 12c) will replace the $C_\perp$ phase with the blocks of star polymer gradually expelled from the surfaces, finally to be a parallel structure, because $C_\perp$ costs too much elastic energy to wet the surface. When the attractive effect of the wall on component A ($HN > 0$) increases further, the structure is mainly occupied by the C block to form an LC1 hybrid structure or an L8 lamellae structure with two A-rich wetting layers in the polymer films. Meanwhile, intermediary perforated lamellae PL3 (Figure 12a,b) emerges as a concomitant in this transition course. The fraction of the chain segment of block C is 0.4, which is larger than the fraction of the other two segments in the whole polymer system;

(50) Brown, G.; Chakrabarti, A. *J. Chem. Phys.* **1994**, *101*, 3310–3317.
(51) Karim, A.; Singh, N.; Sikka, M.; Bates, F. S.; Dozier, W. D.; Felcher, G. P. *J . Chem. Phys.* **1994**, *100*, 1620–1629.
(52) Liu, Y.; Zhao, W.; Zheng, X.; King, A.; Singh, A.; Rafailovich, M. H.; Sokolov, J.; Dai, K. H.; Kramer, E. J. *Macromolecules* **1994**, *27*, 4000–4010.
(53) Harrison, C.; Park, M.; Chaikin, P.; Register, R. A.; Adamson, D. H.; Yao, N. *Macromolecules* **1998**, *31*, 2185–2189.

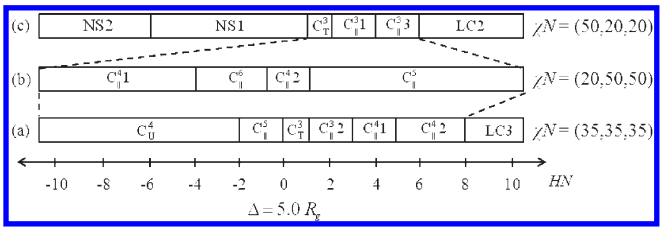

Figure 14. Morphology stability regions for $A_{0.3}B_{0.3}C_{0.4}$ star triblock copolymer thin films as a function of the surface field (HN) at $\Delta = 5.0R_g$ for different series of interaction parameters among components (a) χN = (35, 35, 35), (b) χN = (20, 50, 50), and (c) χN = (50, 20, 20). Squares indicate the range of each kind of morphology as shown in Figures 1−4. The dashed lines indicate the structural transition between cylindrical and noncylindrical phases.

therefore, block C more easily maintains its original structure of a parallel cylinder enriched near the surface and results in an apparently parallel preference for blocks A and B. It is a purely entropic effect. When the repulsive effect of the wall on A component ($HN < 0$) increases, the cylindrical phases ($C_\perp$and $C_{||}$) also disappear and are completely replaced by the perforated lamellae structures (PL) without any other structure, which obviously requires the structural transition of C−PL. As the strength of the surface field increases, different noncylindrical structures are obtained; for example, the $C_{||}$ phase tends to be transformed to PL6 in Figure 12a, and the $C_\perp$ phase tends to be transformed to PL3 and PL1 in Figure 12b,c, respectively. The perforated lamellae phases (PL3) occur over a larger range of HN under conditions at which the AB block pair is more favorable than the AC and BC pairs in comparison to other cases of different interaction parameters, as shown in Figure 10b. Although they are both PL structures, there is an obvious distinction between the PL3 and PL1 (or PL6) phases in that the packaging of cylinders in the pores of lamellae layers is completely different. The packaging of cylinders in PL3 is block C, whereas block B packaging is found in the pores of PL1 (or PL6). This is due to the presence of a junction point of the star triblock copolymer, which indicates that it can adapt to the different strengths of the repellent surface field and take an appropriate PL phase.

We further study the effect of surface fields on the phase behavior in relatively thicker film with different thicknesses of $4.5R_g$ and $5.0R_g$. The phase diagrams of confined ABC star triblock copolymer films as a function of HN for two relatively thick films are shown in Figures 13 and 14. They both show the range of the cylindrical structures' shift to higher attractive preference walls (Figures 13c and 14c) and the broadening to a wider range of field strength (Figures 13a,b and 14a,b), in contrast to those of the relatively thinner film (Figure 12). However, there are some subtle difference between Figures 13 and 14. As the film thickness increases, the undulating cylinder phases are gradually replaced by parallel cylinder phases in the strength range of the surface walls: $-2 < HN < 8.0$ and $-2 < HN < 2.5$ for Figure 13a (and Figure 14a) and Figure 13b (and Figure 14b), respectively. We conclude that when the film thickness is greater than a certain value, such as $\Delta \geq 4.5R_g$, the parallel cylinder phase will dominate at various strengths of the surface field and broaden its range of strength. There is a lack of impact of the surface field on the center of the films in this case ($\Delta \geq 4.5R_g$), and the preferential effects of the surface field will be impaired or even inactive.

For the relatively thick film $\Delta = 5.0R_g$, when the strength of the attractive effect of the A component ($HN > 0$) increases further, it displays a C−L transition in which the cylindrical structures transform to hybrid structures (LC2, LC3) mixed into A-rich wetting layers and cylinders (Figure 14a,c). In fact, the cylindrical morphology seldom transitions directly from cylinders to flat lamellae but always occurs gradually. This phenomenon has been noticed, and it was concluded that there are two accompanying separate transitions between $C_{||}$ and L that must be the C−PL and P−L transitions.[54] On the contrary, as the repellent strength ($HN < 0$) increases, the cylindrical structures are replaced by a large range of film strength for hybrid structures as well (Figure 14c); moreover, there is an obvious phenomenon in which a secondary network of block C emerges in these H regions (NS1, NS2) in which the NS1 phase has been reported in the bulk of linear nonfrustrated ABC triblock copolymers.[55] This is because the domain spacing of confined star triblock copolymers is less than that of the bulk structure without any confinement; meanwhile, the influence of the star junction point on the structure period of the film becomes less important within this scale of film thickness.

4. Conclusions

We have employed self-consistent mean field theory (SCMFT) with a pseudo-spectral method to explore the possible morphology of nearly symmetric $A_{0.3}B_{0.3}C_{0.4}$ star triblock copolymers confined between two homogeneous hard substrates.

By systematically varying the film thickness and the interaction parameters between different species in the star triblock copolymers, phase diagrams are evaluated for the typical block−substrate interactions. To take the preferential effects into consideration, we compare the phase diagrams for weak and strong substrate preferences and discuss the confinement, substrate preference, and nature of the star triblock copolymer effect on the stability of various film phases. Furthermore, the influences of the preferred strength on the film phase are studied on the basis of the different film sizes. The main conclusions are summarized as follows.

Various structures of confined films are found to be stable and are arranged by class: perpendicular cylinders ($C_\perp$), parallel cylinders ($C_{||}$), undulating cylinders (C_U), lamellae (L), perforated lamellae (PL), and hybrid structures (H).

Within neutral walls, the phase diagram shows an alternation between the undulating cylinder (C_U) and nonundulating cylinder (especially for parallel cylinders) for the symmetric interaction parameters (Figure 6a). Under weak preferences, several lamellae structures (L1−L3) with surface-wetting layers can be found in the thinner films (Figures 7b and 8b) because the surface field is strong enough to overpower the entropic energy and then to create two A wetting layers close to and parallel to the substrates. Under strong preferences, the parallel and nonparallel cylinder structures alternately emerge with an oscillating morphology transformation, especially for the thicker films (Figures 9a,b and 10) in this work. For the strongly attractive preference (Figure 9), with increasing film thickness, the lamellae structures gradually transform to parallel cylinder structures, whereas for the strongly repellent preference (Figure 10), the PL structure (PL1−PL4, PL6) occurred only in thinner polymer films because the driving force from the constraint of the star junction point can match the thickness of the film and can flexibly control the appearance of the PL phase.

Contrasting with the thicker film (Figure 13c), the results of the field strength influencing the morphology of relatively thinner films (Figure 12) show that the $C_\perp$ phase appears in small repeat

(54) Huinink, H. P.; van Dijk, M. A.; Brokken-Zijp, J. C. M.; Sevink, G. J. A. *Macromolecules* **2001**, *34*, 5325–5330.
(55) Tyler, C. A.; Qin, J.; Bates, F. S.; Morse, D. C. *Macromolecules* **2007**, *40*, 4654–4668.

parameters (Δ/P_i (i = 1, 2, 3)) because of the weak substrates' preference but is not exclusively determined by the thickness of the film. Moreover, when the film thickness is $\Delta \geq 4.5R_g$, the parallel cylinder phase will dominate under confinement with a broader range of field strength because the preferential effects of the surface field have been released by the relatively thick film itself. We observed an obvious C−PL structure transition in the thinner film, and the hybrid phase with a network structure (NC, NS1, NS2, and LCNS) always appears within a broad H region because the free-energy values of these phases are too similar to be distinguished from one another.

Acknowledgment. We gratefully acknowledge financial support from the National Basic Research Program of China (grant no. 2005CB623800). H.Z. acknowledges support from the National Natural Science Foundation of China (NSFC, grant no. 20874019). F.Q. is grateful for financial support from the NSFC program (grant nos. 20990231 and 20625413).